Electrochimica Acta 485 (2024) 144127

Contents lists available at ScienceDirect

Electrochimica Acta

journal homepage: www.journals.elsevier.com/electrochimica-acta

Unlocking room temperature formation of Li-rich phases in aluminum anodes for Li-ion batteries

Tianye Zheng [a,b,*], Jia Zhang [a], Xiaoyang Guo [c], Wei Jin [a,b], Steven T. Boles [c,*]

[a] Department of Electrical and Electronic Engineering, The Hong Kong Polytechnic University, Hung Hom, Kowloon, Hong Kong
[b] Photonics Research Institute, The Hong Kong Polytechnic University, Hung Hom, Kowloon, Hong Kong
[c] Department of Energy and Process Engineering, Faculty of Engineering, Norwegian University of Science and Technology (NTNU), Trondheim, Norway

ARTICLE INFO

Keywords:
Aluminum Anodes
Li-rich Phases
Nucleation
Lithiation
Kinetics

ABSTRACT

Aluminum (Al) has been an attractive anode candidate for lithium-ion batteries (LIBs) since the 1970s. While the formation of β-LiAl is considered the origin of the Li storage capability in Al anodes, multiple Li-Al phases are known to exist which have even greater lithium content, and the most enriched phase offers twice the theoretical specific capacity of the β-LiAl phase (ca. 2,000 mAh g^{-1}-Al). These Li-rich phases are often neglected in the field of electrochemical energy storage since they are generally believed to be only approachable at elevated temperatures. Here, we demonstrate for the first time that both Li_3Al_2 and $Li_{2-x}Al$ can readily form at room temperature, but only under extraordinarily slow rates, proving that their formation is largely kinetically limited. Although Li_9Al_4 also seems to exist, experimental evidence suggests that its formation is governed by a different mechanism than the other higher-ordered phases. With the constant interplay between diffusion and nucleation, we set out to map the behaviors of Al anodes at different temperatures and rates considering the formation of Li_3Al_2 and $Li_{2-x}Al$. Also, systematic impedance spectroscopy is employed to shed light on the kinetical properties of these two phases, which seem very different from the well-studied β-LiAl, explaining why they were largely neglected in the field of LIBs. While these investigations are mostly consistent with earlier studies, further material characterizations are warranted to better understand how to utilize these Li-rich phases strategically, such that they may be employed in novel lithium-ion cells.

1. Introduction

Tracing back the history of Li-ion batteries (LIBs), the very first wave of anode studies included aluminum (Al) and its alloys. These were initiated in the early 1970s as a replacement and alternative for Li-metal anode to resolve the dendrite issues but were mostly (although not completely) abandoned due to the poor cycling performance. Efforts were made to understand the failure mechanisms of Al anode until the emergence and popularity of the graphite one [1–10], which boosted the commercialization of modern LIBs in the early 1990s. Although a few papers were published from the early 2000s to the end of 2010s, Al anodes are considered largely neglected if compared with their Si or Sn counterparts. Given that utilization of pure alloy anodes remains challenging, commercial efforts tend to focus on graphite-Si blends with Si contents usually less than 20 % [11,12]. On a lab scale, inclusions of other (in-)active elements like Cu or Cr seem another feasible alternative [13,14]. Owing to the unsatisfactory performances of pure alloy anodes, there is a resurgence of interest in reevaluating old alloy anode candidates for higher capacities and improved performance. Interestingly, it appears that a second wave of curiosity into Al anodes may be emerging as solid-state cells look for alternatives to graphite[15].

Recent investigations (i.e., after 2019) on Al anodes include but are not limited to: electrolyte effects [16,17], phase transformations [18,19], lithiation kinetics [20,21], electrode reversibility [22–25], mechanical stresses [23–26], SEI engineering [27–29], prelithiation methods [30–32], electrode stability in air [33,34], and Li solubility of β-LiAl [35–37]. It should be noted that Al foils, among all electrode geometries, are of primary interest due to multiple advantages, such as the omittance of Cu foil and the 'zero volt' stability at high potential vs. Li/Li^+ which is thought to be an advantage for Na-ion batteries [38]. Importantly, the projected fabrication of Al foil anodes should be significantly simplified in the absence of mixing-baking-evaporation processes that are labor-intensive and energy-consuming [39,40]. Considering the breadth of recent research works that cover almost

* Corresponding authors.
E-mail addresses: darren.ty.zheng@connect.polyu.hk (T. Zheng), steven.boles@ntnu.no (S.T. Boles).

https://doi.org/10.1016/j.electacta.2024.144127
Received 13 December 2023; Received in revised form 22 February 2024; Accepted 18 March 2024
Available online 18 March 2024

every facet of the Al anodes in LIBs, several review papers on the topic can be found [10,41], as well as benchmarks for cell performance [42] and electrode design guidance [37].

Regardless of which research motivations are in the above-mentioned studies, the origin of Li storage in Al stems from the phase transformations between α-Al and β-LiAl, thus yielding a well-adopted specific capacity of ~993 mAh g^{-1} considering the ideal 1:1 Li-to-Al ratio or ~1152 mAh g^{-1} upon the formation of $Li_{1.160}Al$ (i.e., saturated β-LiAl) [35]. However, from the binary Li-Al phase diagram [5], there exist multiple Li-rich phases beyond the β-LiAl, namely, Li_3Al_2, $Li_{2-x}Al$, and Li_9Al_4 [43], yielding much higher specific capacities of ~1490 mAh g^{-1}, ~1986 mAh g^{-1}, and ~2234 mAh g^{-1}, respectively [10]. As compared to the β-LiAl, these phases are rarely explored in the LIB field and thus remain poorly understood. We attribute this situation to the fact that they are believed to be only approachable at elevated temperatures [44,45], beyond the perceived limits for a commercial LIB with LP series electrolyte. The recommendations from the limited literature seem to agree that the unsuccessful formation of the Li-rich phases at room temperature is most likely caused by sluggish kinetics, which can be improved by increasing the temperature and decreasing the lithiation rate [45]. In the most recent era, this was evidenced by Ghavidel et al. 2019 where it was found that the formation of Li_3Al_2 and $Li_{2-x}Al$ becomes approachable at low and moderate rates when the temperatures are above 35 ℃ and 60 ℃, respectively [44]. The highest lithiated phase Li_9Al_4, however, seems to be governed by a different mechanism, requiring a temperature of at least 100 ℃. Similarly, a different study demonstrated that either a higher temperature or a lower lithiation rate can facilitate the formation of Li_3Al_2 and $Li_{2-x}Al$ [45]. However, the role of these two factors (i.e., temperature and lithiation rate) in governing the formation of the Li-rich phases, or in general, affect the behavior of Al anodes remains somewhat of a mystery.

Consequently, this study sets out to electrochemically investigate the Li_3Al_2 and $Li_{2-x}Al$ phases, in addition to the well-studied β-LiAl. The exploration of Li_9Al_4 is strategically limited not only due to the fact that the safe operating temperature of LIBs is typically below 65 ℃ but also because the risk of Li dendrite formation becomes higher if Li_9Al_4 is present [32]. By conducting galvanostatic experiments with various lithiation rates and temperatures, the electrochemical behaviors of Al anodes are mapped. Also, electrochemical impedance spectroscopy (EIS) is employed to shed light on the material properties of the different Li-Al phases, based on which, future research directions are recommended.

2. Materials and methods

Electrode preparation and cell assembly. In this work, two kinds of Al electrodes are used: Al thin films and Al foils. The Al thin film electrodes (ca. 1.8 μm thick) on Cu foil substrates were prepared by the magnetron sputtering technique, with the detailed preparation process shown in a previous work [20], while the Al foil electrodes (99.7 %, 30 μm thick) are provided by Toyo Aluminum K.K., Japan. Coin-cells were assembled in an Ar-filled glovebox (≤0.5 ppm H_2O and O_2) with the Al thin film or Al foil disk (12 mm in diameter) as the working electrode and Li metal foil as the counter electrode. Porous glass fiber (Whatman®) was used as the separator and organic electrolytes composed of lithium hexafluorophosphate (1 M $LiPF_6$) salt and carbonate solvent are used, including EC:PC=1:1 vol% and in EC:EMC=3:7 vol%.

Electrochemical characterization. All the electrochemical measurements were carried out using an electrochemical workstation (Bio-Logic, VMP300), namely galvanostatic charge-discharge (GCD) and electrochemical impedance spectroscopy (EIS). The GCD tests were performed on the Al thin film electrodes at four different temperatures: Room temperature (25 ℃), 40 ℃, 50 ℃, and 60 ℃. The cycling rate covered ~C/40, ~C/20, ~C/10, and ~C/5 at each temperature (considering the theoretical capacity of β-LiAl) and the voltage window was between 0.001 V and 1.5 V vs. Li/Li^+. The EIS tests were performed on the cells with Al foils as electrodes when the targeted lithiation depth was reached (i.e., after forming β-LiAl, Li_3Al_2, $Li_{2-x}Al$ phases). The metallic Al foil was selected for the EIS tests to rule out the influence of the Cu substrate if cracks are formed (i.e., Cu exposes to the electrolyte) due to the volume expansion during lithiation. To largely guarantee the reliability of the measured impedance, the cells were held in an open circuit configuration for at least 2 h to reach their equilibrium potentials after each lithiation process. The impedance of the sample at each state was measured under 10 mV perturbation amplitude in the frequency range of 100 kHz to 5 mHz at different temperatures.

Material characterization. The structural information of the fully lithiated Al foil electrode was characterized by X-ray diffraction (XRD) using a Rigaku SmartLab 9 kW diffractometer with Cu Kα radiation at 5°/min in the 2θ angle range of 20°−80°. The Li-Al sample for XRD measurement was obtained by disassembling the coin cell that underwent a lithiation to 100 mV at C/50 followed by a slower lithiation to 1 mV at C/1000. To minimize the air contamination, the sample was sealed using Kapton tape in the Ar-filled glovebox before being placed into the XRD chamber. SEM (Zeiss Merlin) was used to acquire images under an acceleration voltage of 6 kV, using a detector for backscattered electrons (i.e., BSE detector), such that the β phase distribution will be revealed by a reduction in intensity under the grey scale.

3. Results and discussion

The obtained galvanostatic profiles are mapped out systematically under various lithiation temperatures and rates (Fig. 1) For instance, the galvanostatic profile at the upper right corner (i.e., 12.5 μA, 60 °C) clearly exhibits three distinct lithiation plateaus, corresponding to the formation of β-LiAl, Li_3Al_2, and $Li_{2-x}Al$. As the temperature decreases and/or the lithiation rate increases, we observe the merging and eventually the disappearance of the last two plateaus. This merging indicates the simultaneous formation of both Li_3Al_2 and $Li_{2-x}Al$ [45]. When the temperature or lithiation rate does not fulfill the required levels, we anticipate the exclusive formation of β-LiAl, which largely explains why it is widely regarded as the final product of Al anodes in LIBs [10]. In general, Fig. 1 depicts that a higher temperature or a lower lithiation rate seems to yield the equivalent effect on the formation of the Li-rich phases.

Another noteworthy feature in Fig. 1 is the nucleation potentials at various temperatures and lithiation rates. A lower overpotential for nucleating β-LiAl (i.e., a higher potential dip indicated by arrows) is required when the temperature is higher and/or the lithiation rate is lower. Although β-LiAl is not the primary focus of this work, these nucleation potentials seem to be correlated with the formation of the Li-rich phases. Therefore, we first discuss this nucleation potential prior to diving into the Li-rich phases.

3.1. Correlation of β-LiAl nucleation and Li-rich phases formation

With the classical theory of nucleation clearly describing the extra energy required for initiating a phase transformation [46], the nucleation of β-LiAl in an electrochemical cell is indicated by the potential dip at the beginning of the galvanostatic discharge curve (Fig. 1). This amount of overpotentials in Al anodes was firstly defined by Wang et al. 2008 as the 'nucleation potential' [47]. The nucleation process is worth noting since other alloy anodes, such as Si and Sn, do not seem to exhibit evident nucleation barriers during lithiation [48]. Multiple studies have shown that impurities would efficiently reduce this nucleation potential of β-LiAl, such as small additions of Cu [47] Si [18,40] and Fe [49]. Other studies suggest that mechanical work deforming the surrounding α-Al [18] and/or the slow Li diffusion in α-Al [20] could also be responsible for the temporary dip in potential.

Fig. 2a extracts all potential dips from the temperature-rate experiments (i.e. arrow annotations in Fig. 1), which are translated into the nucleation potentials following Fig. 2b. Fig. 2c illustrates that the β-LiAl

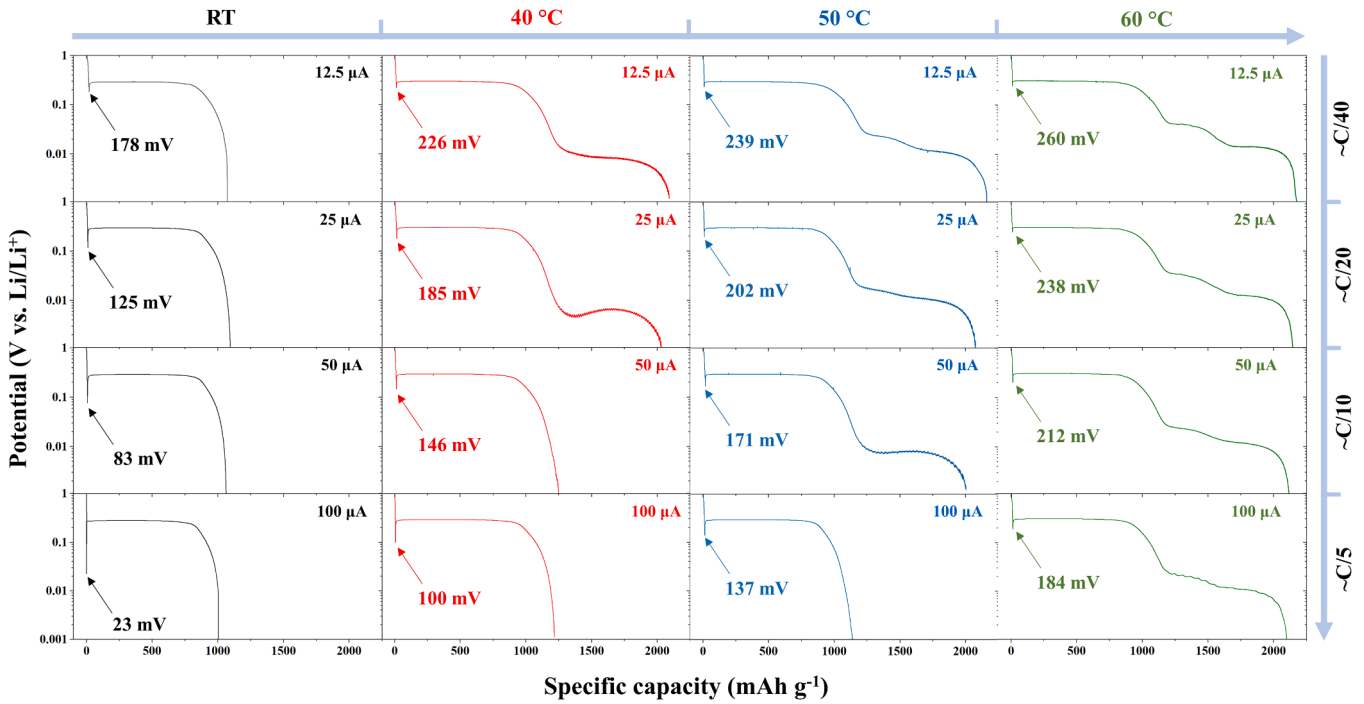

Fig. 1. Galvanostatic discharge profile of Al thin film electrodes at various lithiation rates and temperatures, where the nucleation potentials for the formation of β-LiAl are recorded. The columns from left to right are the data obtained at room temperature (black), 40 °C (red), 50 °C (blue), and 60 °C (green). The rows from top to bottom are the data obtained at ~C/40, ~C/20, ~C/10, and ~C/5, considering the β-LiAl capacity.

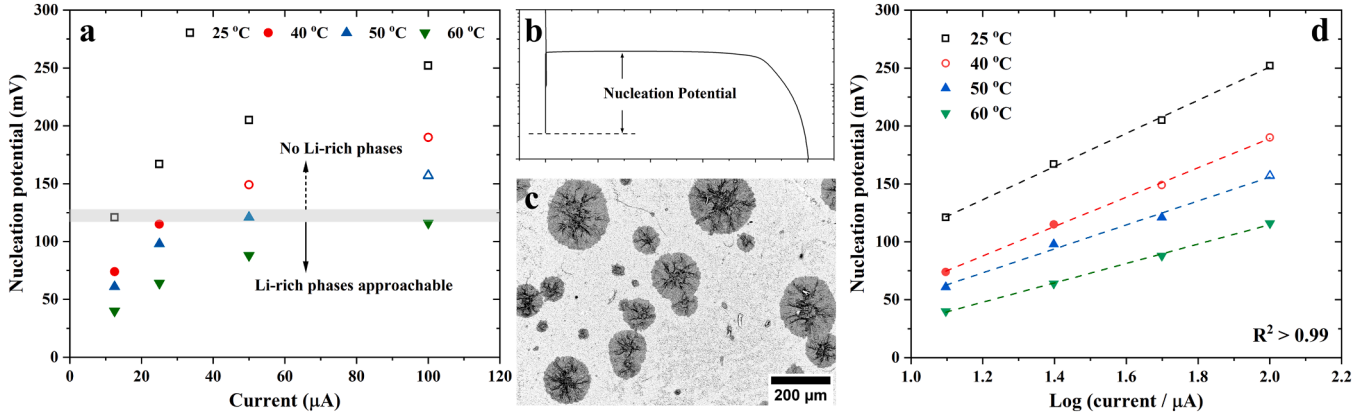

Fig. 2. (a) Nucleation potential as a function of lithiation current under various temperatures for the Al thin film samples. The calculation/definition of nucleation potential is illustrated in (b), and the quantitative data are provided in Table S1. The SEM image in (c) visualizes the nuclei distribution of an Al thin film electrode after partial lithiation. (d) Nucleation potential as a function of the logarithm of lithiation current (the Tafel equation) under various temperatures, where strong linearities are observed.

nuclei are randomly distributed (darker patches due to a lower electron density) in a partly lithiated Al film, which will subsequently expand and merge until the end of lithiation [20]. Taking a closer look, the nucleation potentials presented in Fig. 2a seem to be correlated to the formation of the Li-rich phases. Regardless of lithiation rates and temperatures, the Li-rich phases are formed when the nucleation potential is lower than ca. 120 mV vs. Li/Li^+ that can be translated to 11.6 kJ mol^{-1} using Nernst equation, i.e., $\Delta G^* = nFE^*$, where E^* is the nucleation potential and ΔG^* is the Gibb's free energy when a Li atom is adsorbed to the surface rather than presents in the supersaturated electrolyte [50]. The Tafel equation can be used to model this nucleation process: $\eta = a + b\log i$, where η is the overpotential and i is the current with the empirical constants a, b [51]. As described, in an interfacial kinetical system, the current is often exponentially correlated to the overpotential. This correlation is further supported by the data in Fig. 2d, where the logarithm of the current exhibits strong linearity ($R^2 > 0.99$) against the nucleation potential (i.e., overpotential).

While only a handful of works have elaborated on this nucleation of β-LiAl [47,52], in-depth analysis is beyond the scope of this work. If the β-LiAl nucleation can be precisely projected for Al electrodes under various operation conditions, this suggests that it is then possible to strategically predict whether the Li-rich phases can be accessed based on operational conditions and application purposes. But of course, further studies are warranted in this regard.

3.2. *Incremental capacity analysis (ICA) of the Galvanostatic profiles*

As far as the authors are aware, there are only two recent publications that focus on these higher-order Li-Al phases in the LIB field, namely Ghavidel et al. [44] and Zheng et al. [45]. The following section

aims to shed light on the electrochemical characteristics of the Li-rich phases in Al anodes, by conducting systematic analyses.

Fig. 3 presents the differential capacity curves of the galvanostatic profiles reported in Fig. 1. The β-LiAl peaks of the dQ/dV curves (i.e., the ones at ca. 0.3 V vs. Li/Li^+) are only moderately affected by the different temperatures and lithiation rates. The potential of β-LiAl peak at room temperature and 12.5 μA is 0.291 V, which then shifts to 0.302 V at 60 °C at the same lithiation rate, or to 0.278 V at 100 μA at the same temperature. It should also be noted that the lithiation rate does not seem to play a crucial role when the temperature is sufficiently high, i.e., 60 °C. This non-obvious potential shift is most likely a result of the superior Li diffusion in the β-LiAl. Zhang et al. [13] reported a Li diffusivity of ca. 10^{-7} cm^2 s^{-1} at room temperature in the β-LiAl [37], which may further improve at higher temperatures.

In agreement with most LIB Al anode studies, no Li-rich phases are observed at room temperature, regardless of the lithiation rate. This largely explains why the literature on Al anodes often considers β-LiAl as the end product upon lithiation and 993 mAh g^{-1} as the theoretical capacity [10]. Similar to Ghavidel et al. [44], the extra lithiation peaks corresponding to the formation of Li-rich phases are observed at temperatures slightly above ambient, yet they seem to exhibit kinetic limitations due to their merging and/or shift at the low potential regime. Fig. 3 provides a series of quantitative data that highlight the lithiation peak positions of both Li_3Al_2 and/or $Li_{2-x}Al$. From right to left, at 60 °C, the formation of Li-rich phases is observed at all lithiation rates. The peak position of Li_3Al_2 correlates with the lithiation rates, moving from 0.044 V to 0.019 V, as the lithiation current increase from 12.5 μA to 100 μA. While the peak position of $Li_{2-x}Al$ generally follows the same trend (0.01 V at 100 μA to 0.014 at 25 μA), the $Li_{2-x}Al$ peak seems to split at a slower rate of 12.5 μA. Whether or not this peak splitting is associated with the formation of the Li_9Al_4 is still questionable, especially since this highest Li-Al phase was reported to be only approachable at temperatures beyond 100 °C [44].

When the temperature drops, the overall trend of the peak shift remains, i.e., a higher temperature or a low rate shifts the lithiation peaks towards a higher level. Nevertheless, the Li-rich phases start to become inaccessible at relatively higher lithiation rates, e.g., 100 μA and 50 μA at 50 °C and 40 °C, respectively. No sign of Li_9Al_4 (e.g., a peak splitting) can be observed at these two temperatures (2nd and 3rd columns in Fig. 3). Interestingly, a peak merging is observed at 50 °C, 50 μA (3rd row, 3rd column in Fig. 3) and at 40 °C, 25/50 μA (1st and 2nd rows, 2nd column in Fig. 3). A previous study suggests that this merging is a result of the simultaneous formation of both Li_3Al_2 and $Li_{2-x}Al$ because the potential is sufficiently low and the overall capacity matches that of the

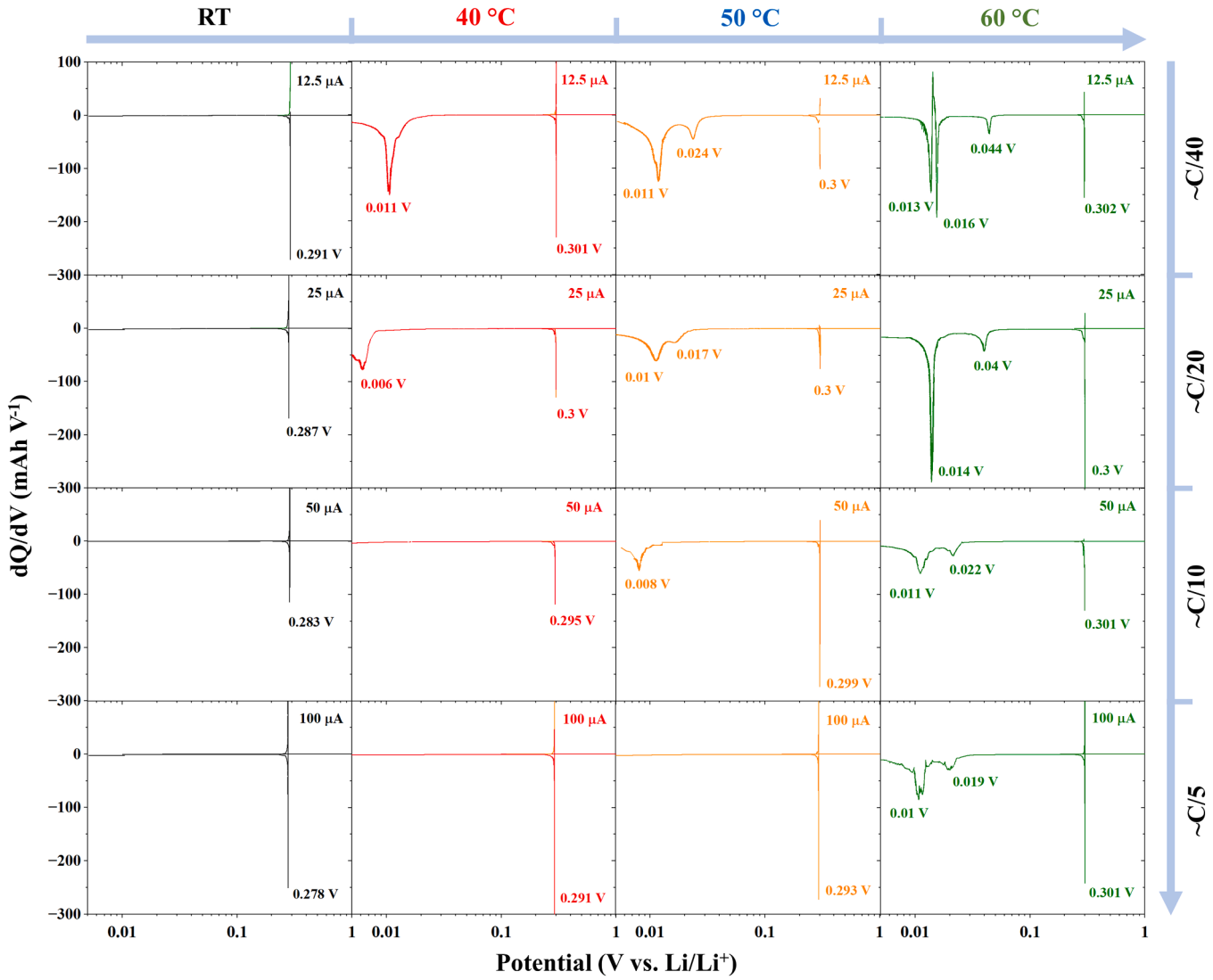

Fig. 3. Incremental capacity analysis (ICA) of the galvanostatic lithiation profiles presented in Fig. 1 (Al thin films). The lithiation peaks, corresponding to the lithiation plateaus in Fig. 1, are annotated. The columns from left to right are the data obtained at room temperature (black), 40 °C (red), 50 °C (blue), and 60 °C (green). The rows from top to bottom are the data obtained at ~C/40, ~C/20, ~C/10, and ~C/5, considering the β-LiAl capacity.

$Li_{2-x}Al$ [45]. The formation of Li_3Al_2 is more heavily affected by the temperature and rate than that of $Li_{2-x}Al$, suggesting different kinetic behaviors between the two phases.

To summarize, these systematic analyses suggest that kinetic barriers could exist during the formation of the Li-rich phases, especially since a lower lithiation current seems advantageous at a given temperature. Through viewing Fig. 1 and Fig. 2, it is hypothesized that the Li-rich phases should be accessible at room temperature if the lithiation rate is sufficiently low.

3.3. Formation of li-rich phases at room temperature

To examine whether the formation of Li-rich phases is approachable at room temperature, a unique galvanostatic lithiation of Al thin film is collected at an extraordinarily slow rate (i.e., 1.5μA), which took ~800 h for a full lithiation (Fig. 4a). This is, to the authors' knowledge, the first successful demonstration of the electrochemical formation of Li-Al phases beyond β-LiAl at room temperature. The obtained specific capacity is slightly higher than 2000 mAh g^{-1}, likely upon the formation of $Li_{2-x}Al$ (i.e., 1986 mAh g^{-1}) considering the charge contributed by SEI growth, doubling that of β-LiAl (i.e., 993 mAh g^{-1}). This finding proves that the formation of Li-rich phases is kinetically limited rather than thermodynamically limited. Zheng et al. 2023 have determined these Li-rich phases to be largely Li_3Al_2 and $Li_{2-x}Al$ for Al thin film electrodes, while the formation of Li_9Al_4 remains unclear [45]. Consequently, the community may view Al anodes differently in the field of LIBs, taking into account the specific capacities of ~1986 mAh g^{-1} or even 2234 mAh g^{-1} upon the formation of $Li_{2-x}Al$ or Li_9Al_4, respectively [10]. As a result, one can distinguish different regimes during the lithiation of Al anodes, including nucleation of β-LiAl [47], coexistence of α-Al/β-LiAl [20,23], solubility range of β-LiAl [35–37], and Li-rich phases [45]. To summarize, the whole picture of Al anodes in Fig. 4a is presented alongside an adapted Li-Al phase diagram (Fig. 4b), such that the capacity and the formation of each phase can be better depicted. The mismatch of the β-LiAl solubility range between Fig. 4a and 4b should be noted, which may be caused by the localized nucleation of Li_3Al_2 when the overall β-LiAl is not fully saturated.

It is suggested that the noise observed on the plateaus in addition to the β-LiAl should be associated with the mechanical strain caused by the volume expansion and the Li diffusion in $Li_3Al_2/Li_{2-x}Al$: Mechanically, Li et al. 2020 reported that the formation of β-LiAl (ca. 95 % larger lattice volume than that of α-Al) [37] could already result in huge mechanical strain locally, thereby plastically deforming the surrounding Al grains [26]. With even larger lattice volumes of $Li_3Al_2/Li_{2-x}Al$, this amount of

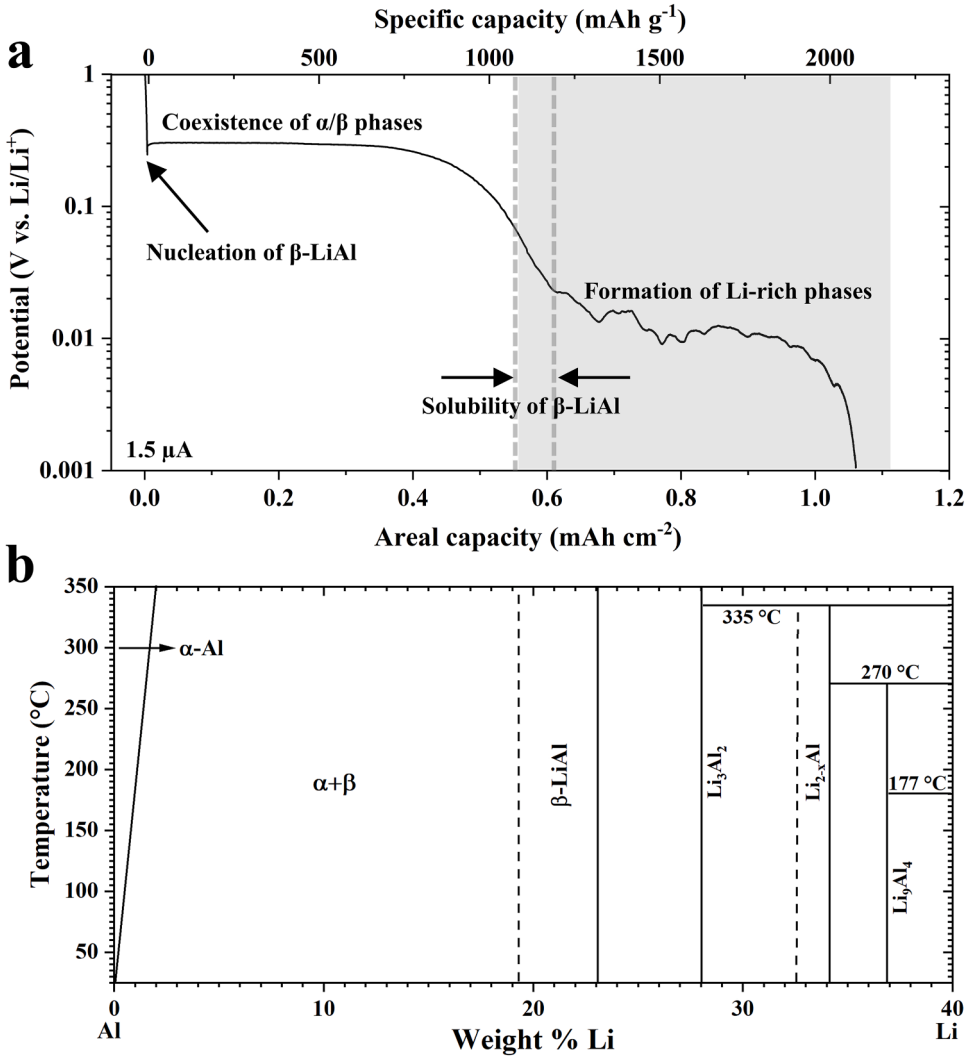

Fig. 4. (a) Galvanostatic discharge profile of an Al thin film electrode (~1.8 μm thick) sputtered on a Cu foil current collector obtained at room temperature. An extraordinarily low current is used, which is equivalent to ~C/400 and ~C/800 (1.5 μA), considering the theoretical capacities of β-LiAl and $Li_{2-x}Al$, respectively. The different lithiation regimes are annotated. The shaded area represents the portion that is often neglected by the scientific community. (b) Partial Li-Al phase diagram (adapted from [10]) is plotted alongside (a) for a clear depiction of the relationship between the capacity and the formation of each phase.

mechanical energy may become problematic and is suggested to be responsible for the noisy potential profile in Fig. 4 (shaded area). It is reported that Li would prefer to insert into regions that are mechanically deformed (e.g., dislocations) due to a chemical potential gain [26], thus shifting the surface potential of the Al electrode and causing unstable surface potentials. Also, Li_9Al_4 is suggested to be thermodynamically unstable and may decompose to Li and $Li_{2-x}Al$ [53]. This process could certainly result in potential noises due to different chemical potentials of Li, Li_9Al_4, and $Li_{2-x}Al$. The unstable nature may prevent Li_9Al_4 from being utilized as a reliable battery anode because the Li_9Al_4 content could vary in each lithiation and during rest. As a result, the $Li_{2-x}Al$ should be considered the end product of Al anodes in LIB applications.

In general, electrochemical kinetic information of these phases can hardly be found since they are generally believed to be only accessible at elevated temperatures and are excluded from the discussions in LIBs. While we suggest a slower Li diffusion in $Li_3Al_2/Li_{2-x}Al$ than that in β-LiAl, further investigations are certainly necessary.

3.4. Structural information of Li-rich phases at room temperature

X-ray diffraction (XRD) was employed to determine the physical structure of the Li-rich phases formed at room temperature. The lithiation is then repeated using a 30 μm thick Al foil, not only to rule out the distraction from the Cu foil substrate of the Al thin films but also because Al foils might be attractive for some applications [29,39,42,54]. Due to the extraordinarily long time required for room temperature lithiation, we have developed a strategic protocol that could shorten the lithiation period by nearly half. As demonstrated in Fig. 5a, the formation of β-LiAl can be relatively quick owing to the fast Li diffusion [37]. The current is then adjusted to be significantly smaller to facilitate the formation of Li-rich phases when the electrode potential reaches ca. 50 mV vs. Li/Li^+, at which the Li_3Al_2 may start nucleating. In this way, the whole lithiation took ca. 1050 h instead of ca. 2000 h.

Like the GCD profile of the Al thin film in Fig. 4a, a noisy potential plateau is also observed in the regime where Li-rich phases are forming, perhaps due to the same reasons elaborated above or simply caused by the non-linear logarithmic y-axis that magnifies the measurement errors. To examine whether the noise is associated with Li_9Al_4 formation and/or Li deposition, the lithiated Al foil then underwent an XRD test. Surprisingly, the diffractogram shown in Fig. 5b exhibits the diffraction peaks of Li_9Al_4 while the existence of $Li_{2-x}Al$ and Li_3Al_2 cannot be ruled out. For instance, the two distinct peaks observed between 25° and 30°

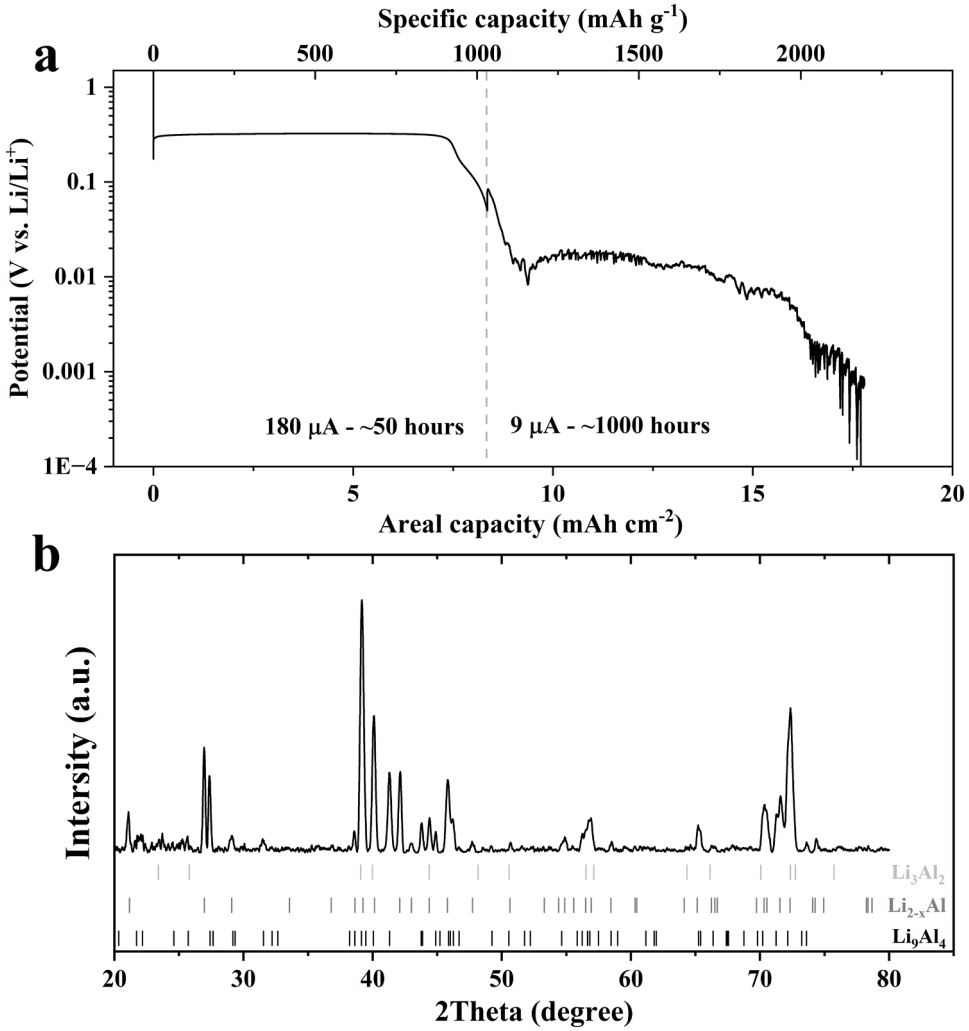

Fig. 5. (a) Galvanostatic discharge profile of a metallic Al foil electrode (30 μm thick) obtained at room temperature. A moderate current (180 μA) is used to form β-LiAl while an extra low current (9 μA) is used to form Li-rich phases. The lithiation rates are equivalent to ~C/50 and ~C/1000, respectively, considering the theoretical capacities of β-LiAl. (b) X-ray diffractogram obtained from the sample in (a). PDF cards #26–1008 (Li_3Al_2), #01–079–8685 ($Li_{1.92}Al_{1.08}$), and #24–0008 (Li_9Al_4) are used as references. Another x-ray diffractogram with a non-significantly different peak distribution was obtained from an Al foil that underwent a full lithiation 50 °C (Figure S1), suggesting that the structural information of these Li-rich phases is not markedly different within the temperature range selected in this study.

may probably refer to Li_9Al_4 while the strong peaks near 40° can be contributed by $Li_{2-x}Al$ and Li_3Al_2, suggesting co-existence of the three phases. The peaks of both α-Al and β-LiAl are absent, meaning that the Li-rich phases are growing at the expense of β-LiAl. The outcome of the XRD test is inconsistent with the conclusion that the formation of Li_3Al_2/$Li_{2-x}Al$ and Li_9Al_4 necessitate temperatures of at least 35 °C and 100 °C, respectively [44]. Although the formation of Li_9Al_4 is reported to be governed by a different mechanism other than that of Li_3Al_2 and $Li_{2-x}Al$ [45], the kinetic barrier also seems to largely explain its absence under regular cycling conditions at room temperature. Otherwise, the coexistence of Li_3Al_2/$Li_{2-x}Al$/Li_9Al_4 should not have been observed in Fig. 5b by solely slowing down the lithiation rate. Furthermore, Kim et al. 2019 found that Li deposition tends to occur around the Li_9Al_4 nuclei, partly explaining why the noisy plateau (if caused by the Li_9Al_4 formation) at the end of lithiation (Fig. 5a) is markedly close to 0 V vs. Li/Li^+ [32]. Li_9Al_4 is reported to be thermodynamically unstable above certain temperatures, which may decompose to form $Li_{2-x}Al$ and Li-rich melt [43]. This decomposition process may alter the surface potential, likely resulting in noisy potential profiles.

The inconsistency between the Al thin film and the Al foil electrode should be acknowledged as well. The former only seems to form $Li_{2-x}Al$ at the end of lithiation while Li_9Al_4 is also detected in the latter, as evidenced by the XRD results. We note that the lithiation rate of the Al foil electrode (~C/1000) is slower than that of the Al film (~C/400), such that Li_9Al_4 might tend to present in the former considering the sluggish kinetics of the higher ordered phases. In addition, with a substrate-based architecture, a misfit strain is anticipated at the interface between the Cu foil substrate and the Al film electrode during lithiation. The compressive stress generated by the volume expansion could shift the potential of the Li_9Al_4 nucleation towards a more negative value [55], which may even be below 0 V vs. Li/Li^+ (i.e., Li deposition over Li_9Al_4 growth). Moreover, the purity of the Al electrode is also suggested to partly affect the accessibility of the Li_9Al_4 phase. According to the classical nucleation theory [46], nuclei tend to initiate and grow at positions where impurities are present. The Al thin films have a purity of 99.9995 % while the Al foils are the commercial 1070 alloy that has ca. 99.7 % purity. The impurities, such as Fe and Si, could readily act as the active sites for nucleating Li_9Al_4.

3.5. Charge transfer resistances of Li-rich phases at various temperatures

To date, the Li-Al phases beyond the β-LiAl remain largely unavailable in the field of electrochemistry. Therefore, EIS is employed in this work to shed light on the electrochemical and kinetic properties of each Li-Al phase growing on Al foils, although more direct material characterization techniques are certainly needed in future studies.

As can be seen from Fig. 6, the ohmic resistances (R_s) are all at a similar level (i.e., the intercept of the x-axis at high-frequency regime), regardless of testing temperatures or Li-Al phases, giving 4.03±0.63 Ω, 3.81±0.46 Ω, 4.18±1.05 Ω, and 3.65 ± 0.61 Ω for the Li-poor, Li-rich β-LiAl, Li_3Al_2, and $Li_{2-x}Al$, respectively. The results suggest that there is no significant difference in electrical conductivity among these Li-Al phases. The charge transfer resistances of all the electrodes can be divided into two regimes: solid-electrolyte interface (SEI, the first semi-circle) and electrochemical double layer (EDL, the second semi-circle), referring to R_{ct} – SEI and R_{ct} – EDL. The quantitative data are extracted from the Nyquist plots in Fig. 6 and summarized in Fig. 7.

As shown in Fig. 7a, generally, these charge transfer resistances contributed by the SEI of different Li-Al phases are higher as the Li content increases, and increasing temperature can effectively reduce the charge transfer resistances. This observation in R_{ct} – SEI can be explained by the electrode potential (Fig. 6), which is lower with higher

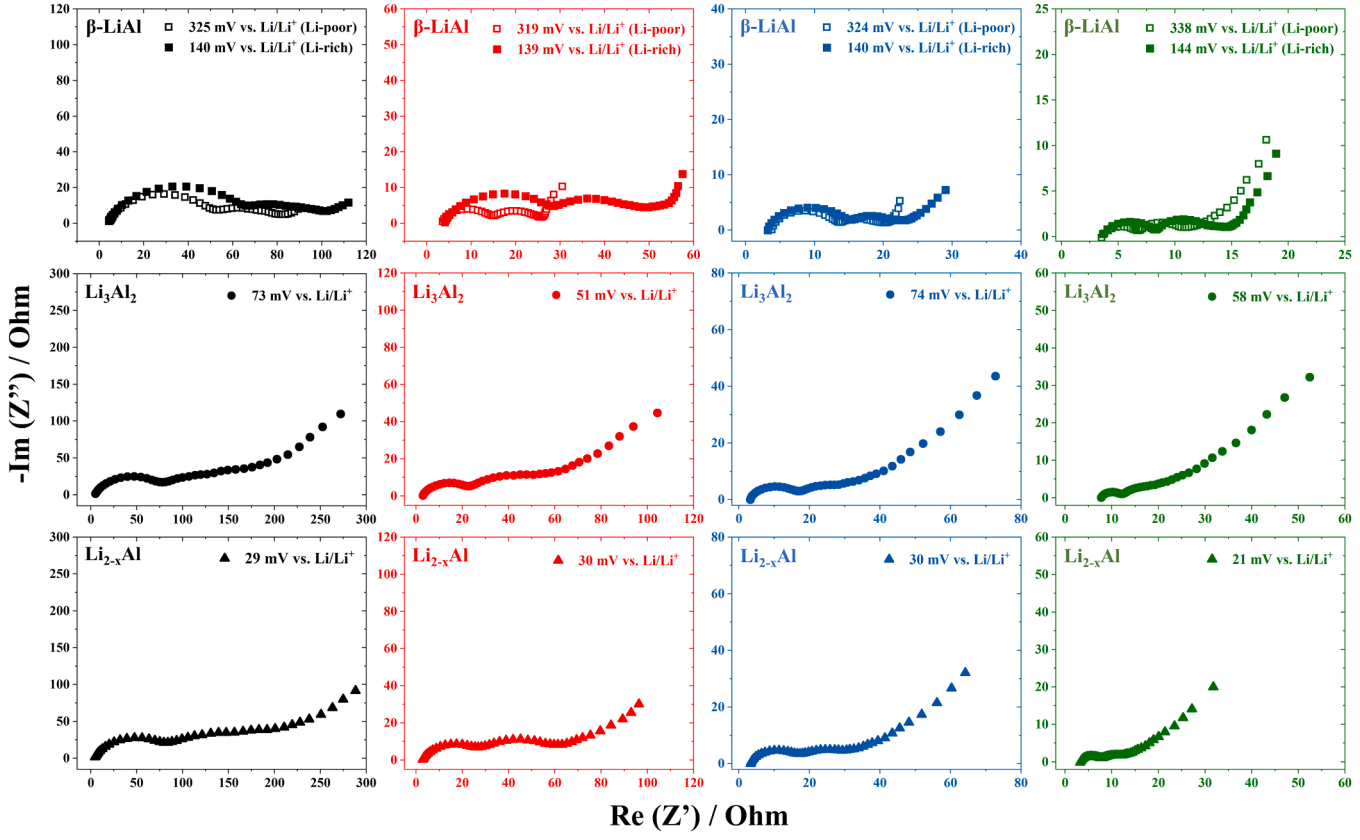

Fig. 6. Electrochemical impedance spectra (EIS) of different Li-Al phases at various temperatures. The columns from left to right are the data obtained at room temperature (black), 40 °C (red), 50 °C (blue), and 60 °C (green). The rows from top to bottom are the data obtained from various Li-Al phases, namely, β-LiAl, Li_3Al_2, and $Li_{2-x}Al$.

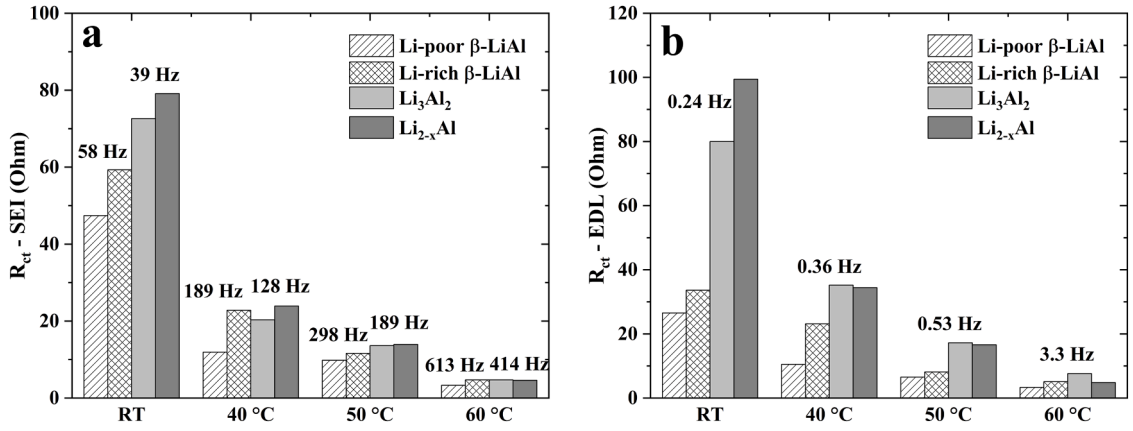

Fig. 7. Data extracted from the Nyquist plots: Charge transfer resistances contributed by (a) solid-electrolyte interface (R_{ct} – SEI) and (b) electric double-layer (R_{ct} – EDL). The quantitative numbers are provided in Table S2.

Li content, thus giving a more pronounced SEI growth (e.g., a thicker SEI).

More specifically, it should be noted that the Li-rich and the Li-poor β-LiAl refer to the Li content of ~53.7 at% for the former and ~47.8 at% for the latter [35]. While maintaining the same crystal structure, the lower electrode potential (or thicker SEI) of the Li-rich β-LiAl (ca. 141±2 mV vs. Li/Li^+) has resulted in a higher R_{ct} – SEI of ~59.3 Ω than that of the Li-poor β-LiAl (~47.4 Ω, ca. 327±7 mV vs. Li/Li^+) at 58.38 Hz alternating potential scans at room temperature. When the temperature increases, the corresponding R_{ct} – SEI values for the two β-LiAl are 22.8 Ω/11.9 Ω – 40 °C, 11.6 Ω/9.8 Ω – 50 °C, and 4.7 Ω/3.2 Ω – 60 °C. The significant reduction of the R_{ct} – SEI values at elevated temperatures indicates that Li ions from the electrolyte can penetrate through the SEI more easily. The first semi-circles in the Nyquist plots fully appear at higher frequencies at higher temperatures, indicating improved kinetics. Likewise, the Li-rich phases also show similar trends because the Li_3Al_2 and $Li_{2-x}Al$ have lower electrode potentials of ca. 64±10 mV and ca. 28 ±4 mV vs. Li/Li^+.

In Fig. 7b, the second semi-circle of the Nyquist plot is suggested to be contributed by the charge transfer in the electrochemical double-layer, e.g., possible dislocations at the grain boundaries. The R_{ct} – EDL values of the β-LiAl phases mostly follow the same trend as the R_{ct} – SEI ones, and the Li-rich β-LiAl has a slightly higher charge transfer resistance at each temperature than the Li-poor β-LiAl. It is reported that the former is dominated by the defects contributed by Li atoms on the Al sublattice while the latter is dominated by the ones contributed by vacancies in the Li sublattice [10]. These vacancies could facilitate a faster ion diffusion, perhaps responsible for a lower R_{ct} - EDL of the Li-poor β-LiAl [5]. As for the Li_3Al_2, the same trend may be briefly explained by the improved kinetics at higher temperatures, giving lower R_{ct} – EDL values.

Significant reductions in the R_{ct} – EDL values of $Li_{2-x}Al$ are observed as the temperature goes up. The value of 99.4 Ω obtained at room temperature drops to 34.4 Ω, 16.6 Ω, and 4.8 Ω, at 40 °C, 50 °C, and 60 °C, respectively. A noteworthy feature is that the R_{ct} – EDL of $Li_{2-x}Al$ at elevated temperatures becomes even lower than that of Li_3Al_2 (it is higher at room temperature), indicating an easier charge transfer of $Li_{2-x}Al$ over Li_3Al_2 at temperatures slightly above ambient. This argument aligns well with the electrochemistry that, within the temperature range from 40 °C to 60 °C (Fig. 1), simultaneous formation of both Li_3Al_2 and $Li_{2-x}Al$ is observed at faster rates. In other words, Li_3Al_2 seems to act as a kinetic barrier in forming the higher-ordered phases beyond the β-LiAl, perhaps due to its higher charge transfer resistance. When the rate is sufficiently low, Li_3Al_2 forms prior to $Li_{2-x}Al$, yielding two plateaus in the GCD profile. The general lithiation process appears to be similar to the sodiation of germanium and can be described by the schematic drawings in a recent study [56].

3.6. Chemical diffusion of Li in Li-rich phases at various temperatures

The low-frequency regime of the EIS Nyquist plot is often controlled by diffusive activities, in our case, the Li diffusion of each Li-Al phase that refers to Walburg impedance or element. According to Ho et al. 1980 [57], the diffusion coefficient can be extracted from the 45° linear region. Both the real and the imaginary impedance should be proportional to the inverse of the square root of frequency (i.e., $\omega^{-1/2}$), which is presented in Fig. 8. To interpret such Warburg plots, attention should be drawn to the slopes and the intercepts based on [58]:

$$Z' = \sigma\omega^{-\frac{1}{2}} + R_S + R_{ct} \quad (1)$$

$$Z'' = \sigma\omega^{-\frac{1}{2}} + 2\sigma^2 C_{dl} \quad (2)$$

where σ is the coefficient of Warburg impedance and C_{dl} is the double-layer capacitance at the electrode surface. Therefore, the slopes of both Eq. (1) and (2) represent the σ value, and they should be parallel. The intercept of Eq. (1) corresponds to the sum of R_s and R_{ct}, which agrees with the values presented in Fig. 7 or Table S2.

In the low-frequency region, the coefficient of Warburg impedance, σ, can be used to determine the chemical diffusion of Li in various Li-Al phases at different temperatures. If assuming a simple 1-dimensional diffusion model, σ can be derived by solving Fick's law of diffusion [57]:

$$\sigma = \frac{V_M(dE/dx)}{\sqrt{2}zFD^{1/2}A} \quad (3)$$

Where V_M is the molar volume of each Li-Al phase, the term dE/dx describes the change in chemical potentials of Li_xAl alloy affected by the alternating voltage amplitude of EIS, $z = 1$ for Li^+ entering the electrode from the electrolyte, F is the Faraday's constant, D is the chemical diffusivity of Li, and A is the electrode area. Assuming the Li concentration in each Li-Al phase is uniform and does not significantly change during the EIS tests, Eq. (3) can be rewritten to obtain the Li diffusivities [57]:

$$D = \left(\frac{V_M}{zFA\sigma}\right)^2 \quad (4)$$

The calculated Li diffusivity values using Eq. (4) are displayed in Fig. 9. As can be seen, the Li diffusivities in the β-LiAl are at a level of 10^{-8} to 10^{-7} cm^2 s^{-1} at all temperatures, agreeing with the previously reported values obtained at room temperature [2,20,37,59]. In the field of metallurgy, it is known that the values would increase as the temperature goes up, e.g., 2.4 × 10^{-6} cm^{-2} s^{-1} at 415 °C and 1.8 × 10^{-5} cm^{-2} s^{-1} at 600 °C [60]. Also, it should be noted that the Li diffusivity of Li-poor β-LiAl is slightly higher than that of Li-rich one, except at 40

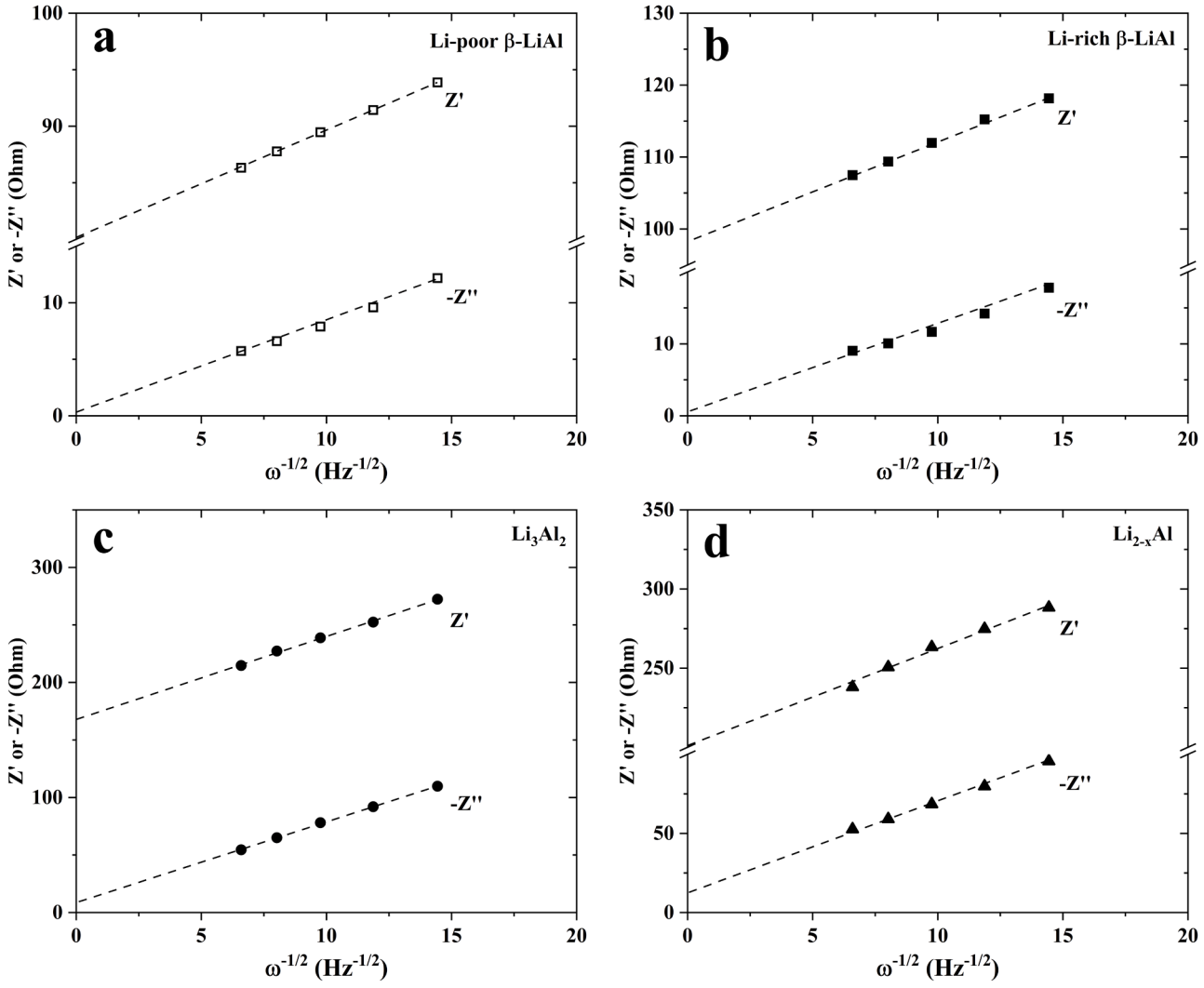

Fig. 8. Real (Z') and imaginary (-Z'') parts of the complex impedance plotted vs. $\omega^{-1/2}$ for (a) Li-poor β-LiAl, (b) Li-rich β-LiAl, (c) Li_3Al_2, and (d) $Li_{2-x}Al$ at room temperature. The data obtained at elevated temperatures are provided in the Supporting Information as Figure S2-S4.

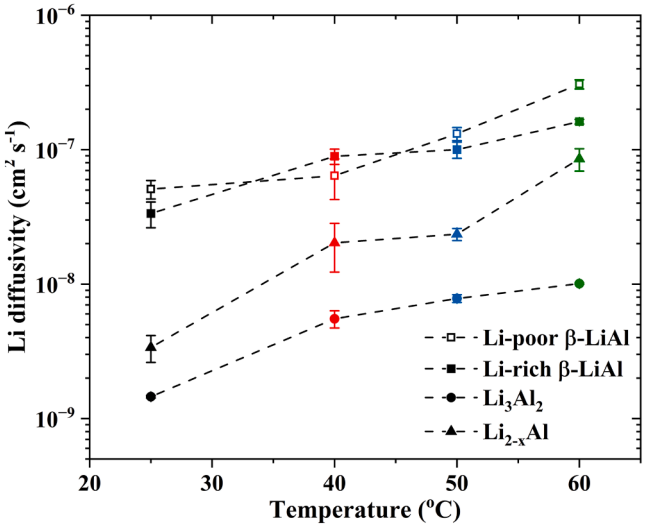

Fig. 9. Li diffusivities within each Li-Al phase calculated from the EIS data obtained at various temperatures. The error bars represent the difference in Warburg coefficients, σ, extracted from the real and the imaginary impedance.

°C, perhaps due to experimental errors. As already mentioned, the vacancies in Li-poor β-LiAl can facilitate faster Li diffusion, thereby resulting in higher *D* values [5].

As anticipated, the Li diffusion in Li_3Al_2 is more than one order of magnitude slower than that in β-LiAl at all temperatures. At room temperature, the Li diffusion of ~1.5×10^{-9} cm^2 s^{-1} in Li_3Al_2 largely explains its inaccessibility, which can also be supported by the observations in other studies [44,45]. Although the Li transportation in Li_3Al_2 becomes faster as temperature increases, it is significantly slower than that in $Li_{2-x}Al$ (~3×10^{-9} cm^2 s^{-1} at room temperature). The Li diffusivity data are consistent with the observation in the GCD profiles that both Li_3Al_2 and $Li_{2-x}Al$ are forming simultaneously (i.e., one extra plateau instead of two, in addition to the β-LiAl one) when the temperature is not sufficiently high, or the rate is not sufficiently low. If compared to popular Si alloy anodes, the Li diffusivities in Li_xAl ($0.916 \leq x \leq 2.25$) are in the same orders of magnitude as the ones in Li_xSi ($1.00 \leq x \leq 3.75$) i.e., 10^{-9} to 10^{-7} cm^2 s^{-1} [61]. This suggests that, at least kinetically, Si anodes should not stand alone as the only promising candidates in the roadmap for future lithium-ion cells.

Fig. 9 also illustrates a monotonic relationship between Li diffusivities in Li_xAl and temperatures, suggesting that higher temperatures should be preferred for the utilization of the Li-rich phases. It should be noted that the analytical method of Warburg impedance may introduce errors in these diffusivity values due to the overlapping of the diffusive-

and the charge transfer-controlled regime [57]. Practically, experimental errors could be inevitable in the coin-type half cells, where the metallic Li foil serves as both the reference and the counter electrode. Therefore, further studies on the kinetic analysis of these Li-rich phases are warranted. A sophisticated 3-electrode or 4-electrode system can be ideal for conducting systematic EIS experiments. At the same time, other electrochemical techniques can also be used to extract the kinetical information of these phases, such as galvanostatic intermittent titration technique (GITT) and/or potentiostatic technique.

4. Conclusions and recommendations

To conclude, this study systematically investigates the electrochemical Li-Al system, highlighting the Li-rich phases beyond β-LiAl. The formation of both Li_3Al_2 and $Li_{2-x}Al$ is demonstrated for the first time at room temperature. This new finding proves that the formation of Li_3Al_2 and $Li_{2-x}Al$ is largely kinetically limited rather than thermodynamically limited. Through analyzing galvanostatic profiles obtained at various temperatures and rates, the formation of Li_3Al_2 and $Li_{2-x}Al$ is found to be facilitated by either a higher temperature or a lower C-rate. A possible correlation between the nucleation of β-LiAl and the accessibility of these phases is observed. Although the X-ray diffractogram seems to support the coexistence of $Li_{2-x}Al$ and Li_9Al_4 in an Al foil electrode that is lithiated at room temperature with an extraordinarily slow C rate, the presence of Li_9Al_4 is suggested to be governed by a different mechanism and thus is excluded from this work. Owing to the scarcity of literature on the Li-rich phases, electrochemical impedance spectroscopy was conducted at various temperatures to shed light on their electrochemical and kinetical properties. While the ohmic resistances of each phase are at a similar level, the charge transfer impedances contributed by the solid-electrolyte interface and by the electrical double-layer follow the sequence of β-LiAl < Li_3Al_2 < $Li_{2-x}Al$ and of β-LiAl < $Li_{2-x}Al$ < Li_3Al_2, respectively. Lastly, the Li diffusivities in each Li-Al phase are extracted from the Warburg region of the Nyquist plot, which nicely agrees with previously reported values. It should be noted that Li_3Al_2 has the slowest Li diffusivity of ca. 1.5×10^{-9} cm^2 s^{-1}. Faster Li diffusion is observed by either removing or adding more Li to form the β-LiAl (ca. 4×10^{-8} cm^2 s^{-1}) or the $Li_{2-x}Al$ (ca. 3×10^{-9} cm^2 s^{-1}) at room temperature. Therefore, the slow Li diffusion in Li_3Al_2 seems to stem from the kinetic barrier in forming the higher-ordered phases beyond the β-LiAl. Increasing temperature can significantly reduce these diffusive impedances and improve Li diffusion, but does not affect the sequence.

The investigations on the Li-rich phases of Li-Al electrodes remain in the early stage, particularly in the field of electrochemical energy storage. Looking forward, multiple characterization means should be beneficial for understanding the material properties of these phases, such as volume/strain changes caused by Li insertion/extraction, mechanical behavior, electrode morphology, and chemical stoichiometry. Given Al's market position as a commodity and structural material, strategical utilization of the Li-rich phases may be best geared towards GWh-scale, long-duration energy storage, or hybrid chemical-electrochemical batteries where chemical refurbishing is warranted by the extraordinary capacities of the active material. Thus, pairings of Al and S or Al and O with Li-ions may offer advantages not seen by other Li-ion chemistries since the extraordinarily slow C rates required for the formation of these phases at room temperature does not seem acceptable in the mainstream LIB field without further optimizations.

CRediT authorship contribution statement

Tianye Zheng: Writing – review & editing, Writing – original draft, Visualization, Methodology, Investigation, Formal analysis, Conceptualization. **Jia Zhang:** Writing – review & editing, Investigation. **Xiaoyang Guo:** Writing – review & editing. **Wei Jin:** Supervision, Funding acquisition. **Steven T. Boles:** Writing – review & editing, Supervision, Resources, Project administration, Formal analysis.

Declaration of competing interest

The authors declare that they have no known competing financial interests or personal relationships that could have appeared to influence the work reported in this paper.

Data availability

Data will be made available on request.

Acknowledgement

T. Zheng would like to acknowledge the "PolyU Distinguished Postdoctoral Fellowship Scheme" (1-YWBT) at The Hong Kong Polytechnic University (PolyU). X. Guo acknowledges the Research Council of Norway for funding under project number 332081 and BEYONDER AS. X. Guo and S. T. Boles would like to acknowledge support from the Research Council of Norway (RCN, Teknologikonvergens Project Number 342109) The authors are thankful to Dr. Diana Avadanii from the IAM-MMI of Karlsruhe Institute of Technology (KIT) for reviewing the paper, and to Dr. Dominik Kramer and Dr. Reiner Mönig from the same institute for the technical discussion. The 180 μm Al foil samples are provided by Toyo Aluminum K.K., Japan.

Supplementary materials

Supplementary material associated with this article can be found, in the online version, at doi:10.1016/j.electacta.2024.144127.

References

[1] N. Yao, L. Heredy, R. Saunders, Emf Measurements of Electrochemically Prepared Lithium-Aluminum Alloy, J. Electrochem. Soc. 118 (7) (1971) 1039–1042, https://doi.org/10.1149/1.2408242.
[2] C.A. Melendres, Kinetics of electrochemical incorporation of lithium into aluminum, J. Electrochem. Soc. 124 (5) (1977) 650–655, https://doi.org/10.1149/1.2133378.
[3] B. Rao, R. Francis, H. Christopher, Lithium-aluminum electrode, J. Electrochem. Soc. 124 (10) (1977) 1490–1492, https://doi.org/10.1149/1.2133098.
[4] J.O. Besenhard, Cycling behavior and corrosion of Li-Al electrodes in organic electrolytes, J. Electroanal. Chem. Interfac. Electrochem. 94 (1) (1978) 77–81, https://doi.org/10.1016/S0022-0728(78)80400-8.
[5] K. Kishio, J.O. Brittain, Defect structure of β-LiAl, J Phys Chem Solids 40 (12) (1979) 933–940, https://doi.org/10.1016/0022-3697(79)90121-5.
[6] E.J. Frazer, Electrochemical formation of lithium-aluminium alloys in propylene carbonate electrolytes, J. Electroanal. Chem. Interfac. Electrochem. 121 (1981) 329–339, https://doi.org/10.1016/S0022-0728(81)80588-8.
[7] T.S. Huang, J.O. Brittain, Effect of defect structure upon the mechanical behavior of β-LiAl through dislocation damping and hardness studies, Metall. Trans. A 13 (12) (1982) 2173–2176, https://doi.org/10.1007/BF02648387.
[8] W. Maskell, J. Owen, Cycling behavior of thin film LiAl electrodes with liquid and solid electrolytes, J. Electrochem. Soc. 132 (7) (1985) 1602–1607, https://doi.org/10.1149/1.2114174.
[9] T.S. Huang, J.O. Brittain, The mechanical behavior of β-LiAl, Mater. Sci. Eng. 93 (1987) 93–97, https://doi.org/10.1016/0025-5416(87)90415-0.
[10] T. Zheng, S.T. Boles, Lithium aluminum alloy anodes in Li-ion rechargeable batteries: past developments, recent progress, and future prospects, Progr. Energy 5 (3) (2023) 032001, https://doi.org/10.1088/2516-1083/acd101.
[11] C.S. Wang, G.T. Wu, X.B. Zhang, Z.F. Qi, W.Z. Li, Lithium insertion in carbon-silicon composite materials produced by mechanical milling, J. Electrochem. Soc. 145 (8) (1998) 2751, https://doi.org/10.1149/1.1838709.
[12] T. Schott, J.L. Gómez-Cámer, P. Novák, S. Trabesinger, Relationship between the Properties and Cycle Life of Si/C Composites as Performance-Enhancing Additives to Graphite Electrodes for Li-Ion Batteries, J. Electrochem. Soc. 164 (2) (2017) A190, https://doi.org/10.1149/2.0701702jes.
[13] X. Zhang, L. Wang, T. Zheng, K.-h. Lam, Synthesis, Electrochemistry, and thermal stability of high-energy ball-milled silicon-based alloy anodes in lithium-ion batteries**, Batter. Supercaps. 6 (5) (2023) e202200495, https://doi.org/10.1002/batt.202200495.
[14] X. Zhang, L. Wang, T. Zheng, K.-H. Lam, Si/CrSi2 alloy anodes synthesized by a high-energy ball-milling method for lithium-ion batteries: microstructure, electrochemistry, and carbon coating, Energy Fuels 37 (15) (2023) 11419–11431, https://doi.org/10.1021/acs.energyfuels.3c01740.

[15] Y. Liu, C. Wang, S.G. Yoon, S.Y. Han, J.A. Lewis, D. Prakash, E.J. Klein, T. Chen, D. H. Kang, D. Majumdar, R. Gopalaswamy, M.T. McDowell, Aluminum foil negative electrodes with multiphase microstructure for all-solid-state Li-ion batteries, Nat. Commun. 14 (1) (2023) 3975, https://doi.org/10.1038/s41467-023-39685-x.

[16] A.K. Chan, R. Tatara, S. Feng, P. Karayaylali, J. Lopez, I.E. Stephens, Y. Shao-Horn, Concentrated electrolytes for enhanced stability of Al-alloy negative electrodes in Li-Ion batteries, J. Electrochem. Soc. 166 (10) (2019) A1867–A1874, https://doi.org/10.1149/2.0581910jes.

[17] B. Qin, S. Jeong, H. Zhang, U. Ulissi, D. VieiraCarvalho, A. Varzi, S. Passerini, Enabling Reversible (De)Lithiation of Aluminum by using Bis(fluorosulfonyl)imide-Based Electrolytes, ChemSusChem 12 (1) (2019) 208–212, https://doi.org/10.1002/cssc.201801806.

[18] M.H. Tahmasebi, D. Kramer, R. Mönig, S.T. Boles, Insights into Phase Transformations and Degradation Mechanisms in Aluminum Anodes for Lithium-Ion Batteries, J. Electrochem. Soc. 166 (3) (2019) A5001–A5007, https://doi.org/10.1149/2.0011903jes.

[19] B. Qin, T. Diemant, H. Zhang, A. Hoefling, R.J. Behm, J. Tübke, A. Varzi, S. Passerini, Revisiting the electrochemical lithiation mechanism of aluminum and the role of Li-rich Phases ($Li_{1+x}Al$) on capacity fading, ChemSusChem 12 (12) (2019) 2609–2619, https://doi.org/10.1002/cssc.201900597.

[20] T. Zheng, D. Kramer, M.H. Tahmasebi, R. Mönig, S.T. Boles, Improvement of the cycling performance of aluminum anodes through operando light microscopy and kinetic analysis, ChemSusChem 13 (5) (2020) 974–985, https://doi.org/10.1002/cssc.201903060.

[21] T. Zheng, X. Wang, E. Jain, D. Kramer, R. Mönig, M. Seita, S.T. Boles, Granular phase transformation of polycrystalline aluminum during electrochemical lithiation, Scr. Mater. 188 (2020) 164–168, https://doi.org/10.1016/j.scriptamat.2020.07.029.

[22] S. Chen, X. Yang, J. Zhang, J. Ma, Y. Meng, K. Tao, F. Li, J. Geng, Aluminum−lithium alloy as a stable and reversible anode for lithium batteries, Electrochim. Acta 368 (2021) 137626, https://doi.org/10.1016/j.electacta.2020.137626.

[23] T. Zheng, D. Kramer, M.H. Tahmasebi, R. Mönig, S.T. Boles, Exploring the reversibility of phase transformations in aluminum anodes through operando light microscopy and stress analysis, ChemSusChem 13 (22) (2020) 5910–5920, https://doi.org/10.1002/cssc.202002023.

[24] P.J. Crowley, K.P. Scanlan, A. Manthiram, Diffusional lithium trapping as a failure mechanism of aluminum foil anodes in lithium-ion batteries, J Power Sources 546 (2022) 231973, https://doi.org/10.1016/j.jpowsour.2022.231973.

[25] Y. Liu, N.S. Hudak, D.L. Huber, S.J. Limmer, J.P. Sullivan, J.Y. Huang, In Situ transmission electron microscopy observation of pulverization of aluminum nanowires and evolution of the thin surface Al_2O_3 Layers during Lithiation–Delithiation Cycles, Nano Lett. 11 (10) (2011) 4188–4194, https://doi.org/10.1021/nl202088h.

[26] H. Li, T. Yamaguchi, S. Matsumoto, H. Hoshikawa, T. Kumagai, N.L. Okamoto, T. Ichitsubo, Circumventing huge volume strain in alloy anodes of lithium batteries, Nat. Commun. 11 (1) (2020) 1584, https://doi.org/10.1038/s41467-020-15452-0.

[27] X. Ou, G. Zhang, S. Zhang, X. Tong, Y. Tang, Simultaneously pre-alloying and artificial solid electrolyte interface towards highly stable aluminum anode for high-performance Li hybrid capacitor, Energy Storage Mater. 28 (2020) 357–363, https://doi.org/10.1016/j.ensm.2020.03.021.

[28] Z. Lu, W. Li, Y. Long, J. Liang, Q. Liang, S. Wu, Y. Tao, Z. Weng, W. Lv, Q.-H. Yang, Constructing a high-strength solid electrolyte layer by In Vivo alloying with aluminum for an ultrahigh-rate lithium metal anode, Adv. Funct. Mater. 30 (7) (2020) 1907343, https://doi.org/10.1002/adfm.201907343.

[29] X. Zhang, W. Zhao, J. Cai, C. Xu, S. Chen, G. Chen, G. Wang, Solid electrolyte interphase layer induced electrochemical behavior diversity of aluminum foil anode for lithium ion batteries, Solid State Ionics 387 (2022) 116081, https://doi.org/10.1016/j.ssi.2022.116081.

[30] J. Ryu, J. Kang, H. Kim, J.H. Lee, H. Lee, S. Park, Electrolyte-mediated nanograin intermetallic formation enables superionic conduction and electrode stability in rechargeable batteries, Energy Storage Mater. 33 (2020) 164–172, https://doi.org/10.1016/j.ensm.2020.08.012.

[31] Y. Yu, S. Li, H. Fan, H. Xu, M. Jiang, Y. Huang, J. Li, Optimal annealing of Al foil anode for prelithiation and full-cell cycling in Li-ion battery: the role of grain boundaries in lithiation/delithiation ductility, Nano Energy 67 (2020) 104274, https://doi.org/10.1016/j.nanoen.2019.104274.

[32] M.S. Kim, S.H.Lee Deepika, M.-S. Kim, J.-H. Ryu, K.-R. Lee, L.A. Archer, W.I. Cho, Enabling reversible redox reactions in electrochemical cells using protected LiAl intermetallics as lithium metal anodes, Sci. Adv. 5 (10) (2019) eaax5587, https://doi.org/10.1126/sciadv.aax5587.

[33] Y. Huang, C. Liu, F. Wei, G. Wang, L. Xiao, J. Lu, L. Zhuang, Chemical prelithiation of Al for use as an ambient air compatible and polysulfide resistant anode for Li-ion/S batteries, J. Mater. Chem. A (2020), https://doi.org/10.1039/D0TA06694J.

[34] H. Fan, S. Li, Y. Yu, H. Xu, M. Jiang, Y. Huang, J. Li, Air-stable LixAl foil as free-standing electrode with improved electrochemical ductility by shot-peening treatment, Adv. Funct. Mater. 31 (29) (2021) 2100978, https://doi.org/10.1002/adfm.202100978.

[35] T. Zheng, D. Kramer, R. Mönig, S.T. Boles, Aluminum foil anodes for Li-ion rechargeable batteries: the role of Li solubility within β-LiAl, ACS Sustain. Chem. Eng. 10 (10) (2022) 3203–3210, https://doi.org/10.1021/acssuschemeng.1c07242.

[36] T. Zheng, S.T. Boles, Simplifying electrode design for lithium-ion rechargeable cells, ACS Omega 7 (42) (2022) 37867–37872, https://doi.org/10.1021/acsomega.2c04966.

[37] J. Zhang, T. Zheng, K.-h. Lam, S.T. Boles, Design considerations and cycling guidance for aluminum foil anodes in lithium-ion rechargeable cells, Electrochim. Acta 456 (2023) 142437, https://doi.org/10.1016/j.electacta.2023.142437.

[38] P. Desai, J. Huang, D. Foix, J.-M. Tarascon, S. Mariyappan, Zero volt storage of Na-ion batteries: performance dependence on cell chemistry!, J. Power Sources 551 (2022) 232177, https://doi.org/10.1016/j.jpowsour.2022.232177.

[39] S.T. Boles, M.H. Tahmasebi, Are Foils the Future of Anodes? Joule 4 (7) (2020) 1342–1346, https://doi.org/10.1016/j.joule.2020.05.009.

[40] S.S. Sharma, P.J. Crowley, A. Manthiram, Aluminum–silicon alloy foils as low-cost, environmentally friendly anodes for lithium-ion batteries, ACS Sustain. Chem. Eng. 9 (43) (2021) 14515–14524, https://doi.org/10.1021/acssuschemeng.1c05168.

[41] H. Wang, H. Tan, X. Luo, H. Wang, T. Ma, M. Lv, X. Song, S. Jin, X. Chang, X. Li, The progress on aluminum-based anode materials for lithium-ion batteries, J. Mater. Chem. A 8 (48) (2020) 25649–25662, https://doi.org/10.1039/D0TA09762D.

[42] T. Chen, A.C. Thenuwara, W. Yao, S.E. Sandoval, C. Wang, D.H. Kang, D. Majumdar, R. Gopalaswamy, M.T. McDowell, Benchmarking the degradation behavior of aluminum foil anodes for lithium-ion batteries, Batter. Supercaps 6 (1) (2023) e202200363, https://doi.org/10.1002/batt.202200363.

[43] K. Puhakainen, M. Boström, T.L. Groy, U. Häussermann, A new phase in the system lithium–aluminum: characterization of orthorhombic Li2Al, J. Solid State Chem. 183 (11) (2010) 2528–2533, https://doi.org/10.1016/j.jssc.2010.08.029.

[44] M.Z. Ghavidel, M.R. Kupsta, J. Le, E. Feygin, A. Espitia, M.D.J.J.o.T.E.S. Fleischauer, Electrochemical Formation of Four Al-Li Phases (β-AlLi, Al2Li3, AlLi2−x, Al4Li9) at Intermediate Temp., 166(16) (2019) A4034–A4040, https://doi.org/10.1149/2.0061916jes.

[45] T. Zheng, J. Zhang, W. Jin, S.T. Boles, Utilization of Li-rich phases in aluminum anodes for improved cycling performance through strategic thermal control, ACS Appl. Energy Mater. 6 (3) (2023) 1845–1852, https://doi.org/10.1021/acsaem.2c03673.

[46] W.D. Callister, D.G. Rethwisch, Materials science and engineering: an introduction, Wiley New York (2018). ISBN978-1-119-40549-8.

[47] C. Wang, Y. Meng, G. Ceder, Y. Li, Electrochemical properties of nanostructured $Al_{1-x}Cu_x$ alloys as anode materials for rechargeable lithium-ion batteries, J. Electrochem. Soc. 155 (9) (2008) A615–A622, https://doi.org/10.1149/1.2943215.

[48] M.N. Obrovac, V.L. Chevrier, Alloy negative electrodes for Li-ion batteries, Chem. Rev. 114 (23) (2014) 11444–11502, https://doi.org/10.1021/cr500207g.

[49] X. Chang, Z. Xie, Z. Liu, X. Zheng, J. Zheng, X. Li, Aluminum: an underappreciated anode material for lithium-ion batteries, Energy Storage Mater. 25 (2020) 93–99, https://doi.org/10.1016/j.ensm.2019.10.027.

[50] Y. Liu, X. Xu, M. Sadd, O.O. Kapitanova, V.A. Krivchenko, J. Ban, J. Wang, X. Jiao, Z. Song, J. Song, S. Xiong, A. Matic, Insight into the critical role of exchange current density on electrodeposition behavior of lithium metal, Adv. Sci. 8 (5) (2021) 2003301, https://doi.org/10.1002/advs.202003301.

[51] O.A. Petrii, R.R. Nazmutdinov, M.D. Bronshtein, G.A. Tsirlina, Life of the Tafel equation: current understanding and prospects for the second century, Electrochim. Acta 52 (11) (2007) 3493–3504, https://doi.org/10.1016/j.electacta.2006.10.014.

[52] Y. Geronov, P. Zlatilova, G. Staikov, Electrochemical nucleation and growth of β-LiAl alloy in aprotic electrolyte solutions, Electrochim. Acta 29 (4) (1984) 551–555, https://doi.org/10.1016/0013-4686(84)87108-X.

[53] The Materials Project. Materials Data on Li_9Al_4 by Materials Project, Berkeley lab, United States, 2020. https://doi.org/10.17188/1274424.

[54] L. Yang, W. Zhao, S. Sun, C. Xu, H. Sun, X. Zhang, G. Wang, Grain boundary density matters in lithiation performances of aluminum foil anode for lithium ion batteries, Mater. Today Commun. 37 (2023) 107179, https://doi.org/10.1016/j.mtcomm.2023.107179.

[55] V.A. Sethuraman, V. Srinivasan, A.F. Bower, P.R. Guduru, In situ measurements of stress-potential coupling in lithiated silicon, J. Electrochem. Soc. 157 (11) (2010) A1253–A1261, https://doi.org/10.1149/1.3489378.

[56] J. Zhang, T. Zheng, K.-w.E. Cheng, K.-h. Lam, S.T. Boles, Insights into the Sodiation Kinetics of Si and Ge Anodes for Sodium-Ion Batteries, J. Electrochem. Soc. 170 (10) (2023) 100518, https://doi.org/10.1016/j.electacta.2023.142437.

[57] C. Ho, I.D. Raistrick, R.A. Huggins, Application of A-C techniques to the study of lithium diffusion in tungsten trioxide thin films, J. Electrochem. Soc. 127 (2) (1980) 343, https://doi.org/10.1149/1.2129668.

[58] M. Shi, Z. Chen, J. Sun, Determination of chloride diffusivity in concrete by AC impedance spectroscopy, Cem. Concr Res. 29 (7) (1999) 1111–1115, https://doi.org/10.1016/S0008-8846(99)00079-4.

[59] A. Baranski, W. Fawcett, The formation of lithium-aluminum alloys at an aluminum electrode in propylene carbonate, J. Electrochem. Soc. 129 (5) (1982) 901–907, https://doi.org/10.1149/1.2124050.

[60] C.J. Wen, B. Boukamp, R.A. Huggins, W. Weppner, Thermodynamic and mass transport properties of "LiAl, J. Electrochem. Soc. 126 (12) (1979) 2258–2266, https://doi.org/10.1149/1.2128939.

[61] Z. Wang, Q. Su, H. Deng, Y. Fu, Composition dependence of lithium diffusion in lithium silicide: a density functional theory study, ChemElectroChem 2 (9) (2015) 1292–1297, https://doi.org/10.1002/celc.201500201.